Interaction of Voids and Nanoductility in Silica Glass

Yi-Chun Chen, Zhen Lu, Ken-ichi Nomura, Weiqiang Wang, Rajiv K. Kalia, Aiichiro Nakano, and Priya Vashishta

Collaboratory for Advanced Computing and Simulations, University of Southern California,
Los Angeles, California 90089-0242, USA

Multimillion-to-billion-atom molecular dynamics simulations are performed to investigate the inter-
action of voids in silica glass under hydrostatic tension. Nanometer size cavities nucleate in intervoid
ligaments as a result of the expansion of Si-O rings due to a bond-switching mechanism, which involves
bond breaking between Si-O and bond formation between that Si and a nonbridging O. With further
increase in strain, nanocracks form on void surfaces and ligaments fracture through the growth and
coalescence of ligament nanocavities in a manner similar to that observed in *ductile* metallic alloys.

When a crack propagates under the influence of an
external load, a part of the mechanical energy is dissipated
ahead of the crack tip in a region called the process zone.
The dissipation occurs through plastic deformation, dam-
age, release of elastic waves, chemical processes, etc. [1].
Classical theories take these mechanisms into account
through phenomenological constitutive relations and dis-
tinguish brittle from ductile and quasistatic from dynamic
fracture [2]. However, experimental studies of the mor-
phology of fracture surfaces for a variety of materials
reveal scaling features that are independent of the precise
nature of the material under consideration or conditions of
loading [3]. This suggests that damage may play a generic
role within the process zone.

Cavitation is a ubiquitous form of damage in the ductile
fracture of metallic alloys [4]. Voids in metallic alloys
nucleate at grain-boundary junctions and from decohesion
or cracking of inclusions [5,6]. Argon *et al.* proposed that
cavities could form if the inclusion diameter is greater than
10 nm and the interfacial stress exceeds a critical value [7].
The growth of an isolated void and various mechanisms by
which voids join in metallic systems have been studied
extensively for many decades [8–13]. Experimental stud-
ies reveal localized, microscopic plastic deformation in
intervoid ligaments prior to coalescence and ligament fail-
ure by microcracking or shearing. In high strength AISI-
4340 steel, ligament failure is observed to be due to the
merging of a sheet of cavities that are an order of magni-
tude smaller than the voids around inclusions [14].

Brown and Embury [15] proposed a simple criterion for
void coalescence in a perfectly plastic material under
tension. According to them, a shear band forms and the
ligament fractures when the void length equals the center-
to-center separation between neighboring voids. Another
criterion for the onset of void coalescence depends criti-
cally on porosity, which is regarded as a material constant
[11]. Simulation studies of void growth and coalescence in
metallic systems have been based mostly on continuum
models [16,17]. Recently, however, molecular dynamics
(MD) simulations have also been used to investigate the

onset of void-void coalescence in copper under hydrostatic
tension [18,19].

In this Letter, we report the results of multimillion-to-
billion-atom MD simulations of void coalescence in an
archetypal brittle material, i.e., silica glass, under hydro-
static tension. A long-held belief is that brittle materials
fracture solely by decohesion of atomic bonds at the crack
tip [20]. However, recent atomic force microscopy (AFM)
studies have generated considerable controversy about the
nature of damage in stress corrosion cracking of brittle
amorphous solids. The Saclay group observes the nuclea-
tion, growth, and coalescence of nanometer scale cavities
as the key mechanism for crack extension in silica and
aluminosilicate glasses [21,22], whereas the NIST group
finds no experimental evidence for cavitation around a
crack in silica glass [23]. Our simulations show nucleation
of nanometer scale cavities in intervoid ligaments, which is
triggered by the coalescence of nearest-neighbor Si-O
rings when a nonbridging oxygen atom binds with silicon
atom and concurrently the latter severs its bond with
another oxygen atom. At higher strains, nanocracks appear
on void surfaces and ligaments fracture due to the growth
and coalescence of ligament nanocavities. Many of these
features in silica glass are surprisingly similar to those
observed in ductile metallic alloys.

Two of the simulations reported here contain 500 voids
in systems with a billion atoms each in a $319.5 \times 296.7 \times 179.7$ nm^3 MD box. In addition, we have investigated
growth and interaction between a pair of voids of varying
sizes and separations in systems with 1×10^6 and 15×10^6 atoms in MD boxes of dimensions $(25.6$ nm$)^3$ and
$(62.8$ nm$)^3$. We impose periodic boundary conditions and
apply a dilatational strain at a constant rate of 10^8 or
10^9 sec^{-1} using the Parrinello-Rahman approach [24].
The equations of motion for the atoms are integrated
with the velocity-Verlet algorithm [25]. Silica glasses are
generated by the melt-quench method described in detail
elsewhere [26]. After preparation, the amorphous systems
are well thermalized at room temperature and spherical
voids are created by removing atoms. These systems with

voids are relaxed with the conjugate gradient method and subsequently heated gradually back to room temperature where they are well thermalized again. Each system with a million atoms was run for 550 ps and each billion-atom system for 120 ps.

All of the simulations are based on an interatomic potential which incorporates ionic and covalent effects through a combination of two-body and three-body terms [27]. The interatomic potential has been validated extensively by comparing the MD simulation results for structural and mechanical properties of amorphous silica (a-SiO$_2$) with experimental measurements [28–31] and quantum mechanical calculations based on density functional theory (DFT). The MD results are in excellent agreement with neutron scattering measurements of static structure factor and with DFT calculations of partial pair-distribution functions and bond angle distributions [32]. The calculated bulk and shear moduli deviate less than 10% from experimental values, and the fracture toughness (1 MPa m$^{1/2}$) also agrees well with experimental results which range between 0.8 and 1.2 MPa m$^{1/2}$ [33].

Figure 1(a) shows the growth of two voids in a million-atom a-SiO$_2$ system. In this simulation the initial diameter of the voids is 3 nm, the center-to-center void separation is 6 nm, and the applied dilatational strain rate is 10^8 sec^{-1}. With an increase in the applied strain, the void diameters grow slowly at first from their initial size of 3 nm to 3.5 nm and when the strain, ε, is about 4% nanometer size cavities nucleate in the intervoid ligament region. In order to delineate damage nucleation and evolution due to void-void interaction from that caused by independent void growth, we have also simulated the growth dynamics of one void under the same initial conditions (1×10^6-atom system with a void of diameter 3 nm) and strain rate (10^8 sec^{-1}).

Figure 1(b) shows the ratio of the average volume per void, ϕ_2, in the system with 2 voids to the void volume in the single-void system, ϕ_1. Up to a strain of about 7%, the average growth rate of two voids is nearly the same as that of a single void but there are no damage cavities in the
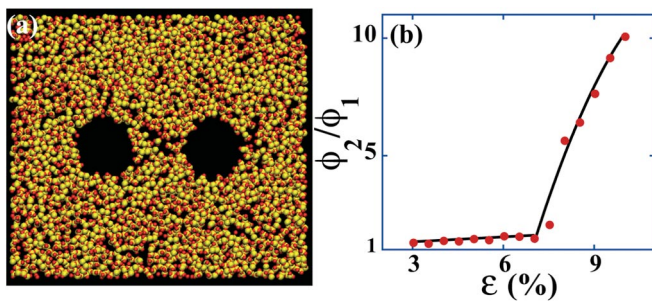
latter system. Starting at a strain of 7%, nanocracks appear on the surfaces of the two voids and their average void growth rate far exceeds the growth rate of a single void; see Fig. 1(b). In the two-void case, intervoid ligament cavities grow and at $\varepsilon = 8\%$ the intervoid ligament fractures due to the coalescence of voids with the nanocavities. At coalescence the intervoid ligament distance is close to the radius of either void, which agrees qualitatively with the Brown-Embury criterion for ductile materials.

To determine the influence of the void-void interaction on structural changes in the intervoid ligament region prior to ligament fracture, we monitor the Si-O pair correlation function, $g_{\text{Si-O}}(r)$, and the Si-O-Si bond angle distribution, $P_{\text{Si-O-Si}}(\theta)$, as a function of the applied strain, ε. Figure 2(a) shows the changes in the first peak in $g_{\text{Si-O}}(r)$ at $\varepsilon = 8\%$ relative to that in the unstrained system. The height of the first peak drops significantly because of the decrease in the coordination of Si resulting from Si-O bond breaking. The height of the second peak in $g_{\text{Si-O}}(r)$ also drops, which indicates changes in the—Si-O-Si-O-Si—ring structure. These changes are also evident in the bond angle distribution $P_{\text{Si-O-Si}}(\theta)$ shown in Fig. 2(b): at $\varepsilon = 4\%$, $P_{\text{Si-O-Si}}(\theta)$ is narrower and shifted to higher angles compared to the unstrained system. At higher values of ε, Si-O bond breaking causes a partial shift in $P_{\text{Si-O-Si}}(\theta)$ back towards the unstrained case.

Detailed analysis of cavity nucleation reveals a novel mechanism involving strain-enhanced defect transport; see Fig. 3(a)–3(c). In the unstrained a-SiO$_2$, each Si atom (yellow) is connected to 4 O atoms (red) and these SiO$_4$ tetrahedra are linked into nanometer size—Si-O-Si-O-Si—rings through corner-sharing O atoms. In Fig. 3(a), blue, green, and gray regions are inside a 7-, 6- and 5-membered Si-O ring, respectively. The blue atom in Fig. 3(a) is a nonbridging O bonded to a Si in the 7-membered blue ring. The oxygen atoms, shown in green and white, play a pivotal role in the nucleation of a nanocavity. Figure 3(b) shows that at a strain of 1% the nonbridging O (blue) becomes fully coordinated by binding with a Si while the white O atom becomes under-coordinated by dissociating from that Si atom. As a result, the 5-membered gray ring becomes a 12-membered ring

FIG. 1 (color). (a) Snapshot of voids and nanocavities at a strain rate of 10^8 sec^{-1}. (b) Strain dependence of the average porosity per void in the two-void system, ϕ_2, relative to the porosity of the single-void system ϕ_1.
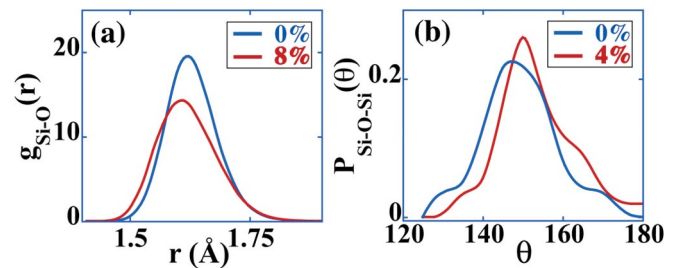

FIG. 2 (color). (a) Si-O pair-distribution functions and (b) Si-O-Si bond angle distributions in the middle of the intervoid ligament in the unstrained and strained systems.
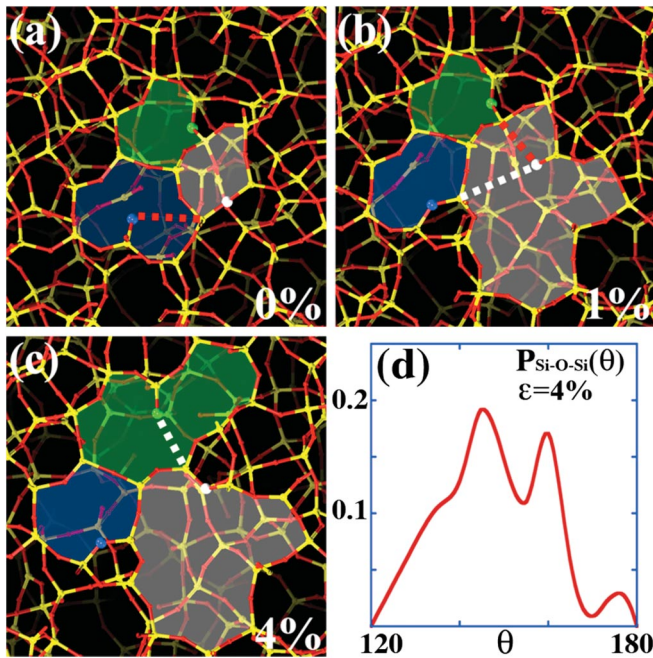
FIG. 3 (color). Bond-switching mechanism involving non-bridging oxygens is shown in (a) and (b) by red and white dashed lines between blue and white atoms. In (c), the white dashed line indicates bond switching between white and green oxygens; (d) shows the Si-O-Si bond angle distribution for the rings involved in the bond-switching events. Yellow and red spheres represent Si and O atoms, respectively.

FIG. 4 (color). Voids in a billion-atom system under a strain rate of 10^9 sec^{-1}. (a) shows a slice of the entire system; (b) shows cracks on void surfaces at $\epsilon = 9\%$; (c), (d) show void coalescence and intervoid ligament failure at $\epsilon = 10.5\%$ and $\epsilon = 12\%$, respectively.

and the blue oxygen is now a part of a 3-membered ring. At a strain of 4%, the green O dissociates from a Si atom and the latter binds with the white O atom, thus creating an 11-membered ring (gray) adjacent to a 10-membered ring (green); see Fig. 3(c). The transport of nonbridging O is driven by stress gradients. This mechanism introduces a natural length scale, i.e., ring diameter (~ 1 nm), into the nanocavity nucleation problem. Figure 3(d) shows a considerable change in $P_{\text{Si-O-Si}}(\theta)$ for the rings with bond-switching events involving nonbridging O: instead of a single broad peak at 143° [Fig. 2(a)], the distribution has another peak at 160° due to strain-induced growth of rings. Void-void coalescence studies in a 15×10^6-atom SiO$_2$ glass at a hydrostatic strain of 10^9 sec^{-1} reveal the same mechanisms for the nucleation and growth of damage nanocavities and intervoid ligament failure.

Figure 4 shows evolution and coalescence among multiple voids in a billion-atom system subjected to a dilatational strain of 10^9 sec^{-1}. The initial configuration is an array of 500 voids distributed at the center of the specimen, about 100 nm from the boundaries in the x and y directions and 60 nm from the boundaries in the z direction; see Fig. 4(a). The initial diameter of each void is 3 nm and the smallest center-to-center void separation is 9 nm. As the strain is increased to 4.5%, sheets of nanocavities nucleate in intervoid ligaments and small cracks appear
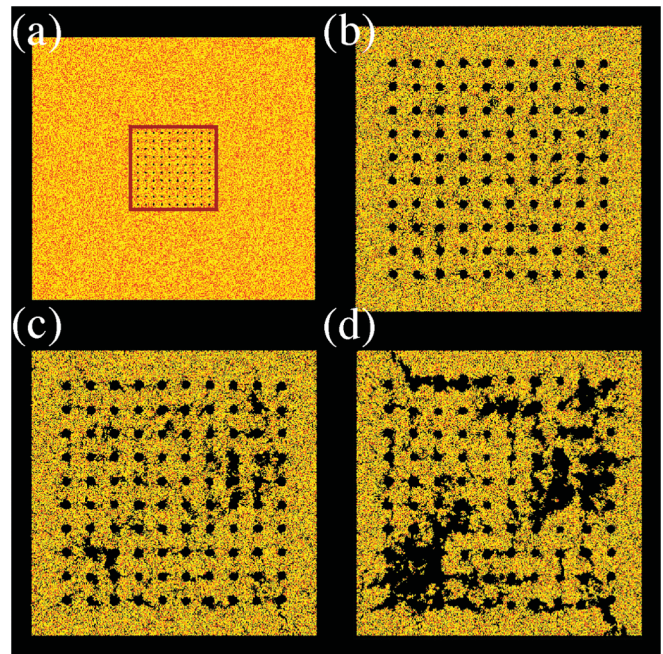
on void surfaces. Nanocavities form in ligaments between nearest neighbor as well as next nearest-neighbor voids (diagonal ligaments). The voids and ligament cavities grow and merge to fracture the ligaments. The ligaments first fail at a strain of 8% around the corner voids. With a slight increase in strain (9%), ligaments between many different voids fracture [Fig. 4(b)]. This releases the tensile stress on voids close to the fractured ligaments and as a result they shrink in size and cracks on their surfaces begin to heal. Figures 4(c) and 4(d) show intervoid ligament fracture and crack formation resulting from the coalescence of many voids at a strain of 12%.

We have also investigated the effect of an applied dilatational strain (at a strain rate of 10^9 sec^{-1}) on a *random* spatial distribution of 500 nonoverlapping voids in a billion-atom a-SiO$_2$ system. The initial size of each void is 3 nm and the void centers are chosen from a uniform random distribution. Figure 5 shows the porosity of this system, and for comparison the porosity of the system with regularly distributed voids, as a function of the applied strain. As the strain is increased, the voids first grow independently of one another without any significant damage around them. However, when the strain exceeds 8% small cracks appear on the surfaces of some voids along with the onset of void coalescence; see Fig. 5(a). The void-void interaction and eventual coalescence are again mediated by the nucleation and growth of intervoid ligament nanocavities. Figure 5(b) shows a mosaic of cracks result-
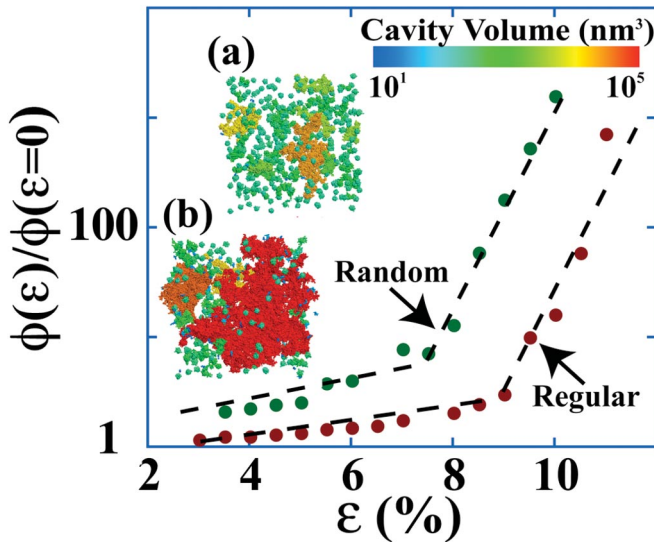
FIG. 5 (color).   Porosity vs strain in billion-atom systems containing 500 identical voids distributed regularly and randomly; (a), (b) show volumes of coalesced cavities in the latter system at $\epsilon = 8\%$ and 10%, respectively.

ing from the percolation of voids through the system at a strain of 10%.

In summary, we have discovered that damage nanocavities in a-SiO_2 arise from the migration of nonbridging oxygen atoms in—Si-O-Si-O-Si—rings and that these nanocavities play an important role in void-void coalescence and intervoid ligament failure. Interestingly, Mott proposed the same mechanism for flow in silica glass [34]. It should be possible to experimentally verify our predictions regarding void-void interaction and coalescence by sculpting nanovoids in a silica membrane with a transmission electron microscope shirking technique [35] then subjecting the membrane to hydrostatic tension. Such experiments have been performed in the case of metals by laser drilling holes [36].

[1] S. Yip, *Handbook of Materials Modeling* (Springer, New York, 2005).
[2] F. F. Abraham *et al.*, Europhys. Lett. **44**, 783 (1998).
[3] E. Bouchaud, Surf. Rev. Lett. **10**, 797 (2003).
[4] V. Tvergaard *et al.*, Eur. J. Mech. A. Solids **11**, 215 (1992).
[5] F. M. Beremin, Metall. Trans. A **12**, 723 (1981).
[6] B. J. Lee and M. E. Mear, J. Mech. Phys. Solids **47**, 1301 (1999).
[7] A. S. Argon *et al.*, Metall. Trans. A **6**, 825 (1975).
[8] V. Tvergaard, Adv. Appl. Mech. **27**, 83 (1990).
[9] B. J. Budianski *et al.*, in *Mechanics of Solids: The Rodney Hill 60th Anniversary Volume* (Pergamon, New York, 1982).
[10] A. C. F. Cocks and M. F. Ashby, Prog. Mater. Sci. **27**, 189 (1982).
[11] A. C. F. Cocks and M. F. Ashby, Metal Science **14**, 395 (1980).
[12] F. A. McClintock, Mech. Eng. Soc. Mech. Eng. **90**, 56 (1968).
[13] J. R. Rice and D. M. Tracey, J. Mech. Phys. Solids **17**, 201 (1969).
[14] T. B. Cox and J. R. Low, Metall. Trans. **5**, 1457 (1974).
[15] L. M. Brown and J. D. Embury, in *Third International Conference on Strength of Metals and Alloys* (Institute of Metals, London, 1973), p. 164.
[16] V. Tvergaard and A. Needleman, Int. J. Solids Structures **32**, 1063 (1995).
[17] S. Ramaswamy and N. Aravas, Comput. Methods Appl. Mech. Eng. **163**, 11 (1998).
[18] E. T. Seppala *et al.*, Phys. Rev. B **71**, 064112 (2005).
[19] E. T. Seppala *et al.*, Phys. Rev. Lett. **93**, 245503 (2004).
[20] B. Lawn, *Fracture of Brittle Solids* (Cambridge University Press, Cambridge, England, 1993).
[21] F. Celarie *et al.*, Phys. Rev. Lett. **90**, 075504 (2003).
[22] D. Bonamy *et al.*, Int. J. Mater. Prod. Technol. **26**, 339 (2006).
[23] J. P. Guin and S. M. Wiederhorn, Int. J. Fract. **140**, 15 (2006).
[24] M. Parrinello and A. Rahman, J. Appl. Phys. **52**, 7182 (1981).
[25] M. P. Allen and D. J. Tildesley, *Computer Simulation of Liquids* (Oxford University Press, Oxford, 1987).
[26] A. Nakano *et al.*, J. Non-Cryst. Solids **171**, 157 (1994).
[27] P. Vashishta *et al.*, Phys. Rev. B **41**, 12 197 (1990).
[28] D. L. Price, Current Opinion in Solid State & Materials Science **1**, 572 (1996).
[29] Q. Wang *et al.*, J. Non-Cryst. Solids **143**, 65 (1992).
[30] J. P. Lucas *et al.*, Scr. Metall. Mater. **32**, 743 (1995).
[31] C. L. Rountree *et al.*, Annu. Rev. Mater. Res. **32**, 377 (2002).
[32] L. Yang has performed a DFT calculation on a configuration generated by our MD simulation. The relaxed structure from the DFT calculation is very close to the MD configuration.
[33] L. Van Brutzel *et al.*, Mater. Res. Soc. Symp. Proc. **703**, V3.9 (2001).
[34] N. F. Mott, Philos. Mag. B **56**, 257 (1987).
[35] A. J. Storm *et al.*, Nat. Mater. **2**, 537 (2003).
[36] A. Week, Ph.D. thesis, McMaster University, 2007.